A Design Study for Thermal Control of a CVD Reactor for YBCO

Martha A. Gallivan, David G. Goodwin, and Richard M. Murray
Division of Engineering and Applied Science
California Institute of Technology
Pasadena, CA 91125
Email: martha@cco.caltech.edu

Abstract

Active thermal control of a reactor for $YBa_2Cu_3O_{7-x}$ chemical vapor deposition is studied using a nonlinear heat transfer model validated by preliminary component testing. LQR and LQE methods are applied to the linearized model for observer-based control. Convergence rates of the controller and observer are indicated by closed-loop eigenvalues and disturbance rejection is assessed with $\mathcal{H}_2$ and $\mathcal{H}_\infty$ norms. Design tradeoffs are quantified with these measures by varying model parameters. Maximum errors in control and estimation for a nominal design case are both 21 K, and longest timescales are 45 seconds and 10 seconds for the controller and observer, respectively.

1. Introduction

Superconducting $YBa_2Cu_3O_{7-x}$ (YBCO) devices have many potential applications, including high-performance microwave filters for cellular communications. However, realizing their potential requires the development of high throughput manufacturing processes to deposit high-quality, uniform films on large substrates. Metalorganic chemical vapor deposition (MOCVD) is one promising technique for YBCO thin film deposition [4]. In an MOCVD process, a heated substrate is exposed to a gas flow containing organometallic precursor molecules, which decompose in the hot boundary layer above the substrate, resulting in film deposition. Since the properties of the film are very sensitive to substrate temperature during growth, good thermal control is vital. A typical requirement for YBCO is a substrate temperature of 1100 K, with uniformity of $\pm$ 3 K over a 2" diameter substrate.

The thermal control issues studied in this work are part of a larger effort to design and build an MOCVD reactor for the deposition of YBCO. The preliminary reactor design is shown in highly simplified form in Figure 1. Gas-phase precursors enter through a showerhead. The magnesium oxide (MgO) substrate is held in a silicon carbide (SiC) susceptor, which sits above an Inconel can containing the graphite heating elements. The susceptor is levitated slightly and rotates due to a gas jet emerging from the can.

Sensing of substrate temperature is one challenge encountered in implementing active thermal control. Because invasive temperature measurement devices disrupt film growth and preclude substrate rotation, the substrate temperature must be measured with non-invasive techniques [10], or inferred through a model-based observer. In this work, an observer is constructed which takes as inputs other reactor temperature measurements to estimate the local, time-varying substrate temperature.

Much work has been done to model and measure reactor heat transfer dynamics in rapid thermal processing (RTP) reactors. While many of the methods may be applicable to the YBCO reactor, previous work has focused primarily on characterization of existing reactors in the initial, pre-growth configuration [1, 3, 9, 5] or with an assumed film growth law [10]. This work quantifies the effect of film growth on the control and estimation of substrate temperature, with no growth law assumed *a priori* in the model-based observer. Film growth is modeled as an external disturbance, and linear feedback control methods are used to assess the reactor's thermal response. Performance sensitivity to design parameters provides input to the reactor design process.

2. Reduced-Order Nonlinear Heat Transfer Model

A wavelength-dependent heat transfer model of the reactor has been developed, which incorporates radiation and conduction. Consideration of the wavelength-dependent radiative effects is critical in accurately modeling the reactor, since the radiative properties of key components vary dramatically with wavelength, and therefore with temperature. Convection heat transfer is neglected due to the low re-

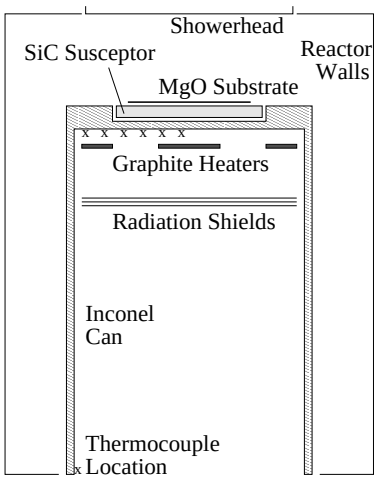

Figure 1: Cutaway view of reactor model.

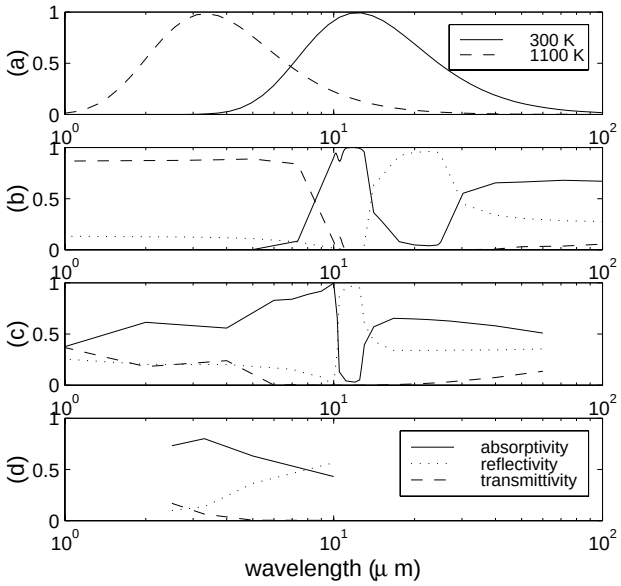

Figure 2: (a) Product of blackbody function and wavelength at 300 K and 1100 K; single-crystal radiative properties of (b) 0.020" MgO (c) 1/8" SiC (d) 0.5 μm YBCO.

actor pressure of 10 Torr.

2.1. Description of Model

To model the radiative heat transfer in the reactor, a set of enclosure equations was written which relates the radiative flux leaving each surface to the incoming flux from all other surfaces. The conduction heat flux was modeled by a finite-difference representation [7].

Wavelength-dependence of radiative heat flux must be included in the model to reflect the dramatic vaiations in radiative properties with wavelength, as shown in Figure 2. As temperature changes, the blackbody curve shifts to smaller wavelengths, changing the overall radiative properties of a surface. These properties were computed from the complex refractive index of each material [6, 8] and the thickness of each component, assuming normal incidence and neglecting interference effects [2]. The enclosure equations were solved and summed over 8 wavelength bands, with different radiative properties associated with each band.

The MgO substrate, the SiC susceptor, and the Inconel can were discretized into concentric rings to obtain a set of ordinary differential equations from the partial differential and integral equations describing conduction and radiation. An energy balance on each ring yields

$$\rho c_p L A_i \frac{dT_i}{dt} = q_{\text{radiation}} + q_{\text{conduction}} + q_{\text{input}} \qquad (1)$$

where ρ is the density, L is the thickness of the disk, and A_i is the surface area of the ring. These energy balances may be combined into a single matrix equation to yield a state-space representation with an extra nonlinear term:

$$\dot{T} = A_1 T + A_4 T^4 + Bu \qquad y = CT, \qquad (2)$$

where u defines the inputs of heater power and constant wall temperature, C is the constant output matrix, and y is the vector of system outputs. It should be noted that the matrices A_1, A_4 and B are not constant since they include temperature-dependent material properties.

Additional heat transfer constraints are also explicitly defined in the model to represent the actual reactor configuration. These constraints include internal resistive power dissipation in the heaters and conduction and radiation boundary conditions.

Equation (2) is integrated with a Runge-Kutta fixed time step scheme. Heater power inputs may be constant or defined by a controller. PID and LQR controllers have been implemented on the model.

2.2. Preliminary model validation

Component testing was undertaken to assess the validity of the heat transfer model and to determine physical constants prior to reactor construction. The experimental setup consisted of a steel can, a SiC susceptor, and a thermocouple-instrumented MgO substrate, as pictured in Figure 3. The heaters were wire resistance coils wound from Kanthal wire. The heater design was later changed to use graphite

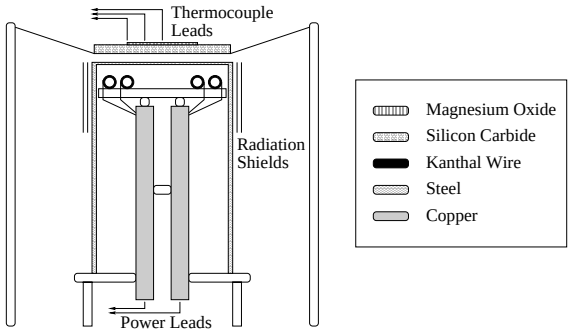

Figure 3: Experimental apparatus for model validation experiment.

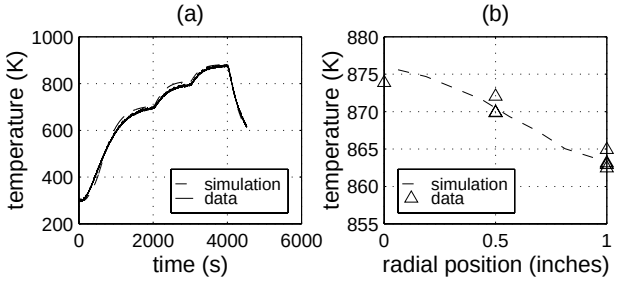

Figure 4: Comparison of data and simulation results: (a) temperature versus time (b) temperature versus radial position.

heaters; however, both types of heaters are modeled as flat rings. The setup was placed in a vacuum chamber to duplicate the modeling assumption of negligible convective heat transfer. The 2" diameter MgO substrate was instrumented with 9 thermocouples.

A simulation was run to duplicate the times and conditions of the experimental data. The maximum temperature achieved during the test was less than the target substrate temperature of 1100 K due to heater failure, but the data were still useful for validating the model. The model parameters were matched to dimensions and material properties of the component test, with unknown parameters, such as the emissivity of oxidized steel and the contact resistance between MgO and SiC, estimated from the data. These parameters were consistent with tabulated values for similar materials. The simulation matches the data in overall temperature magnitude and in temperature gradient across the substrate as plotted in Figure 4.

3. Analysis of Linearized System

Linearization of the nonlinear heat transfer model enables the application of linear feedback control techniques for quantification of errors and design tradeoffs. Since the range of operating points desired during film growth is limited to substrate temperatures between 1000 K and 1200 K, the nonlinear heat transfer model was linearized about a typical operating point corresponding to a substrate temperature of 1100 K. The remaining temperatures were determined from simulations of the full nonlinear model. An 8-ring model was used throughout the study. The state and input matrices, A and B, are constant matrices from the linearization process, and the output matrix C transforms all the states into a vector containing only the states associated with thermocouples on the can. The final linearized system takes the form

$$\frac{d}{dt}(\delta T) = A\,\delta T + Bu \qquad y = C\,\delta T, \tag{3}$$

where $\delta T \in \mathbb{R}^{29}$ consists of the can temperatures, susceptor temperatures, substrate temperatures, and heater temperatures. The input $u \in \mathbb{R}^3$ consists of power inputs and fixed wall temperature.

The two systems of interest describe the natural dynamics of the actual temperature under closed loop control and the error in the estimated temperature:

$$\frac{d}{dt}(\delta T) = (A - BK)\,\delta T \qquad \frac{d}{dt}(e) = (A - LC)\,e. \tag{4}$$

The two linear systems for the controller and observer are considered separately in this study, although they will ultimately be coupled to form the single reactor system. The systems are studied separately to independently assess the effects of design variations on control and on estimation.

The control matrix K and the estimator matrix L are computed with the Matlab functions `lqr` and `lqe`. The eigenvalues of matrices $A-BK$ and $A-LC$ were computed to determine the largest time constants associated with the control loop and the observer loop.

In addition to system time constants, an important consideration in the design of a reactor for growing YBCO on MgO is the disturbance caused by film growth. As YBCO grows on the largely transparent MgO substrate, the substrate surface gradually becomes opaque to incident radiation. In this study, the change in radiative properties of the substrate during growth is viewed as a disturbance acting on the substrate states, and the disturbance rejection performance of the control and observer systems is quantified with $\mathcal{H}_2$ and $\mathcal{H}_\infty$ norms. The $\mathcal{H}_2$ and

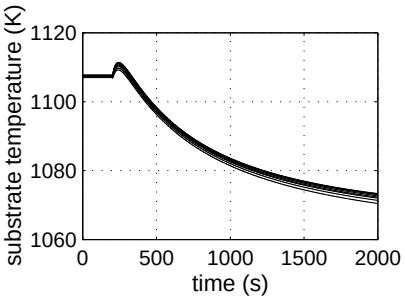

Figure 5: Typical effect of film growth disturbance on substrate temperature under a fixed input, with film growth beginning at 200 s. Curves represent individual substrate states.

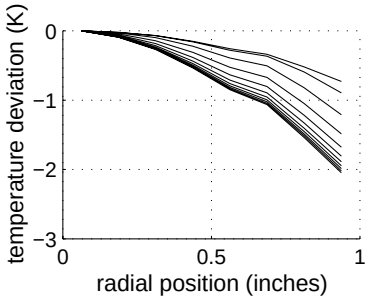

Figure 6: Film growth temperature deviations from operating point normalized by centerline temperatures based on nonlinear simulation. Curves represent substrate profiles at intervals of 100 s.

$\mathcal{H}_\infty$ norms for $A - BK$ and $A - LC$ were computed with the Matlab functions `h2norm` and `hinfnorm` for a range of design parameters to evaluate the effect of design choices on closed-loop performance of the reactor. The disturbance enters into the linear systems as

$$\frac{d}{dt}(\delta T) = (A - BK)\,\delta T + B_1 d \tag{5}$$

$$\frac{d}{dt}(e) = (A - LC)\,e + B_1 d, \tag{6}$$

A zero block in B_1 contains the number of columns equal to the total number of heater, can, and susceptor states, while the identity block is of dimension equal to the number of substrate states. Thus, the disturbance vector d acts independently on each substrate state.

The full nonlinear model was used to simulate the substrate temperature change during film growth with a fixed power supplied to the heaters. These substrate temperatures are shown in Figure 5. Film growth begins at a time of 200 s. The surface of the substrate instantaneously changes from MgO to an infinitesimally thin layer of YBCO. The YBCO layer then gradually thickens to 0.5 μm at 2000 s, where the film growth representation in the model is linear in time. This growth model was used only for the purpose of disturbance estimation. The film growth simulated is typical of known times and thicknesses used in YBCO thin film growth. The disturbance enters the linearized model as a derivative of temperature with time, as in equations (5) and (6). To quantify this typical disturbance d, $\|d\|_2$ is calculated by integrating the derivative of the temperature change associated with each state on the substrate:

$$\|d\|_2^2 = \int_{t_o=200}^{t_f=2000} d^T d\, dt, \tag{7}$$

where

$$d_j = \frac{dT_j^{sub}}{dt}. \tag{8}$$

Implemented on the simulation results at discrete time intervals Δt,

$$\|d\|_2^2 = \sum_{i=1}^{m}\sum_{j=1}^{n} \frac{\Delta T_{ij}^{sub}}{\Delta t}, \tag{9}$$

where m is the number of time steps in the time interval considered and n is the number of states on the substrate. The value of $\|d\|_2$ for the case considered in Figure 5 is 6.12.

The output of the linear systems considered is composed of the temperature and estimation errors of the substrate states. These norms are the products of a transfer function norm and $\|d\|_2$. When $\|\delta T^{sub}\|_\infty$ and $\|\delta T^{sub}\|_2$ are considered for a typical profile shape, a maximum temperature change across the substrate is determined. Typical temperature deviation profiles across the substrate are shown in Figure 6. These profile snapshots are taken at every 100 s throughout the duration of the film growth. The nonlinear simulation shows that as the film grows, the substrate tends to cool faster at the edges. A representative profile of this temperature deviation is a parabolic distribution. When a parabolic distribution is assumed across the substrate, the maximum error in temperature is less than $\|\delta T^{sub}\|_\infty$. For a parabolic profile with no deviation at the center, the ratio of maximum error to $\|\delta T^{sub}\|_\infty$ is 0.7.

The $\mathcal{H}_\infty$ norm may be similarly quantified by considering temperature deviations over a finite time interval. However, it does not represent an absolute bound on temperature deviation from the operating point. While minimizing the $\mathcal{H}_\infty$ norm in the design

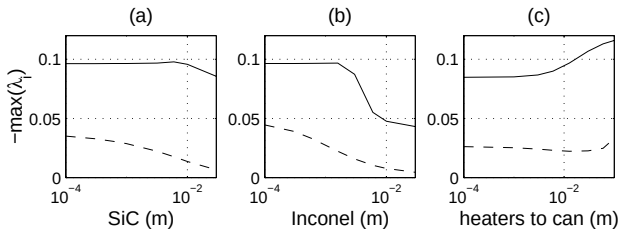

Figure 7: Eigenvalues associated with largest time constant for variations in reactor design parameters: (a) susceptor thickness (b) can thickness (c) distance between heaters and can. Solid lines refer to controller and dashed lines to observer.

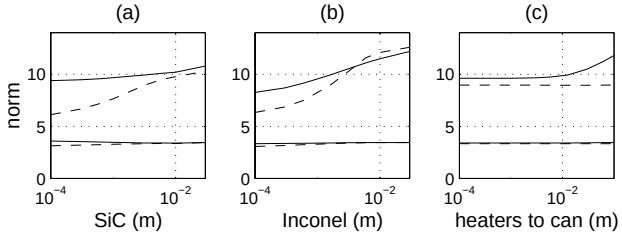

Figure 8: Norms associated with variations in reactor design parameters: (a) susceptor thickness (b) can thickness (c) distance between heaters and can. Solid lines denote control system and dashed lines denote observer. $\mathcal{H}_\infty$ curves are on top and $\mathcal{H}_2$ curves are below.

on the reactor is desirable, no fixed value is considered acceptable or unacceptable.

The time scales and norms defined previously were computed over a range of values for three design parameters: the susceptor thickness, the can thickness, and the distance between the heaters and the can. A nominal design case was selected, with a 1/8" thick susceptor, a 1/16" Inconel can top, and a spacing of 1/2" between the heaters and the can top. The parameters were then varied about the nominal design case. These variations are plotted in Figures 7 and 8. Figure 7 shows the largest eigenvalue associated with both the control and observer systems. It is observed that as thickness of components is increased, both the controller and observer response slow due to increased thermal inertia. Distance between the heaters and can does not affect thermal inertia, although moving the heaters farther from the can enables more uniform heating of the can and quicker response. Figure 8 illustrates the effect of reactor design parameters on disturbance rejection. It is noted that the $\mathcal{H}_2$ norms associated with both the control and observer systems are quite insensitive to all the design parameters studied, but that the $\mathcal{H}_\infty$ norms vary with the chosen design parameters.

	Case A	Case B	Case C
SiC (m)	1×10^{-3}	3.175×10^{-3}	6×10^{-3}
Can (m)	6×10^{-4}	1.5785×10^{-3}	3×10^{-3}

Table 1: Definition of design cases.

Although the plots generally suggest that reduced thermal mass yields improved performance, practical considerations such as machining must also be considered. This parametric study may be included in such practical discussions to identify the feasibility of control for various designs.

Another important consideration in analyzing the parametric study is the assessment of tradeoffs. While Figure 7 indicates that increasing the distance between the heaters and the can improves performance, Figure 8 shows higher error when the heaters are too far from the can. The plots suggest that a desirable distance would be near 1 cm.

Quantifiable bounds on errors in control and estimation for a single set of design parameters is another useful result. For the nominal design case considered, the $\mathcal{H}_2$ norm is 3.41 for the control loop and 3.34 for the observer. A typical value of $\|d\|_2$ associated with film growth was determined to be 6.12, where $\|\delta T\|_\infty$ and $\|e\|_\infty$ are the products of $\mathcal{H}_2$ and $\|d\|_2$. Thus, $\|\delta T\|_\infty$ is 20.9 K and $\|e\|_\infty$ is 20.4 K. The longest time scales associated with the nominal design case may also be determined from this analysis, where 45 s is the longest time scale of the control loop, and 10 s is the longest time scale of the observer system.

4. Nonlinear Simulation Validation of Linearized Results

Variation in performance with design parameters was demonstrated with linear techniques applied to the linearized form of the heat transfer model. Nonlinear simulations may also be used to show similar trends. Three sets of design parameters are chosen to represent designs in which the thermal mass is less than that associated with the nominal set of design parameters (Case A), equal to the thermal mass of the nominal case (Case B), and greater than the nominal case (Case C). The values of the parameters are shown in Table 1. Figure 9 shows the variations in centerline can temperature during film growth for each design case, with growth beginning at a time of 200 s. Because the observer determines substrate temperature based on can temperature, the magnitude of the change in can temperature is also a measure of observability. The linear analysis predicted

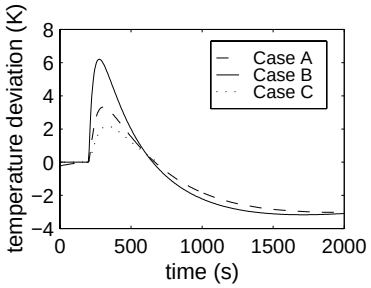

Figure 9: Nonlinear simulations of centerline can temperature during film growth, beginning at 200 s.

that the can would be harder to control and to observe as thermal mass increased. This result is also seen in the nonlinear analysis. The can response associated with Case A is the fastest and of the greatest magnitude throughout the film growth, while Case C shows the slowest and the smallest can response. The nonlinear simulations confirm that lower reactor thermal mass yields faster and greater can response to film growth disturbances.

5. Conclusion

The development of a heat transfer model for an MOCVD reactor enabled the study of control characteristics prior to construction. Experimental data first demonstrated the validity of the model. Linear analysis, including LQR and $\mathcal{H}_2$ methods, provided insight into the control and estimation performance of the reactor under an unknown disturbance acting on the substrate. This disturbance was quantified through examination of film growth in nonlinear simulations of the heat transfer model.

The maximum temperature control errors and estimation errors for a nominal set of design parameters was determined to be 21 K for each system, or 15 K if a parabolic profile was assumed. The largest time scale associated with this controller is 45 seconds, and with this observer 10 seconds. The study suggests that achieving the target ± 3 K uniformity across the substrate requires some knowledge of the film growth, either through the addition of a film growth law to the model or the incorporation of noninvasive temperature measurement of the substrate. Both are promising and are the focus of current work.

A parametric study, varying design parameters and assessing the effect on control and estimation performance, suggested trends and tradeoffs involved in improving closed-loop reactor performance. The performance assessment provided by the heat transfer model and subsequent control analysis contributes to the intelligent design of the reactor.

Acknowledgments

This work is supported in part by DARPA/NSF DMS-9615858, AFOSR F49620-95-1-0419, and an NSF graduate fellowship. We would also like to thank Ashok Tripathi, who built much of the apparatus used in the model validation experiments.

References

[1] Terrence Breedijk, Thomas F. Edgar, and Isaac Trachtenberg. Model-based control of rapid thermal processes. *Proceedings of the American Control Conference*, pages 887–891, 1994.

[2] M. Quinn Brewster. *Thermal Radiative Transfer and Properties.* John Wiley and Sons, Inc., New York, 1992.

[3] Young Man Cho and Paul Gyugyi. Control of rapid thermal processing: A system theoretic approach. *IEEE Transactions on Control Systems Technology*, 5(6):664–653, November 1997.

[4] Aiguo Feng, Ling Chen, Timothy W. Piazza, Hongwen Li, Alain E. Kaloyeros, Drew W. Hazelton, Li Luo, and Robert C. Dye. High-quality Y1Ba2Cu3O7-x thin films on polycrystalline MgO by temperature-controlled chemical vapor deposition. *Applied Physics Letters*, 59(10):1248–1250, September 1991.

[5] Michael Gevelber, Manuel Toledo-Quinones, and Michael Bufano. Toward closed-loop control of CVD coating microstructure. *Materials Science and Engineering*, A209:377–383, 1996.

[6] J. Humlicek, J. Kircher, H. U. Habermeier, M. Cardona, and A. Roseler. Infrared optical-response of YBa2Cu3O7 and PRBa2Cu3O7 - an ellipsometric study. *Physica C*, 190(4):383–395, January 1992.

[7] Frank P. Incropera and David P. DeWitt. *Fundamentals of Heat and Mass Transfer.* John Wiley and Sons, Inc., New York, 1990.

[8] Edward D. Palik, editor. *Handbook of Optical Constants of Solids.* Academic Press, Orlando, 1985.

[9] Charles D. Schaper, Mehrdad M. Moslehi, Krishna C. Saraswat, and Thomas Kailath. Modeling, identification, and control of rapid thermal processing systems. *Journal of the Electrochemical Society*, 141(11):3200–3209, November 1994.

[10] F. Yates Sorrell, Seungil Yu, and William J. Kiether. Applied RTP optical modeling: An argument for model-based control. *IEEE Transactions on Semiconductor Manufacturing*, 7(4):454–459, November 1994.